Construction of a pillararene-based supramolecular polymer network and its application in efficient removal of dyes from water †

Xiaoqing Lv,[a, b] Danyu Xia,*[a] Yujie Cheng,[a, b] Jianbin Chao,[a] Xuehong Wei,*[a], Pi Wang,*[c]

[a]*Scientific Instrument Center, Shanxi University, Taiyuan 030006, P. R. China.*

[b]*School of Chemistry and Chemical Engineering, Shanxi University, Taiyuan 030006, P. R. China*

[c]*College of Materials Science and Engineering, Taiyuan University of Technology, Taiyuan 030024, P.R. China*

Electronic Supplementary Information (23 pages)

1.Materials and methods.

All reagents were commercially available and used as supplied without further purification. Solvents were either employed as purchased or dried according to procedures described in the literature. Compounds **a**[S1] and **H**[S2] was prepared according to published procedures. NMR spectra were recorded with a Bruker Avance DMX 600 spectrophotometer. High-resolution mass spectrometry experiments were performed with a Waters UPLC H-Class QDA instrument. Scanning electron microscopy (SEM) investigations were carried out on a JEOL 6390LV instrument. UV−vis spectra were taken on a SHIMADZU UV−2450 spectrophotometer. The viscosity was recorded with a SYP-256B viscometer. Dynamic light scattering was carried out on a Malvern Zatasizer Nano ZS instrument at room temperature.

*2.Synthesis of compound **1** and model guest compound **G**.*

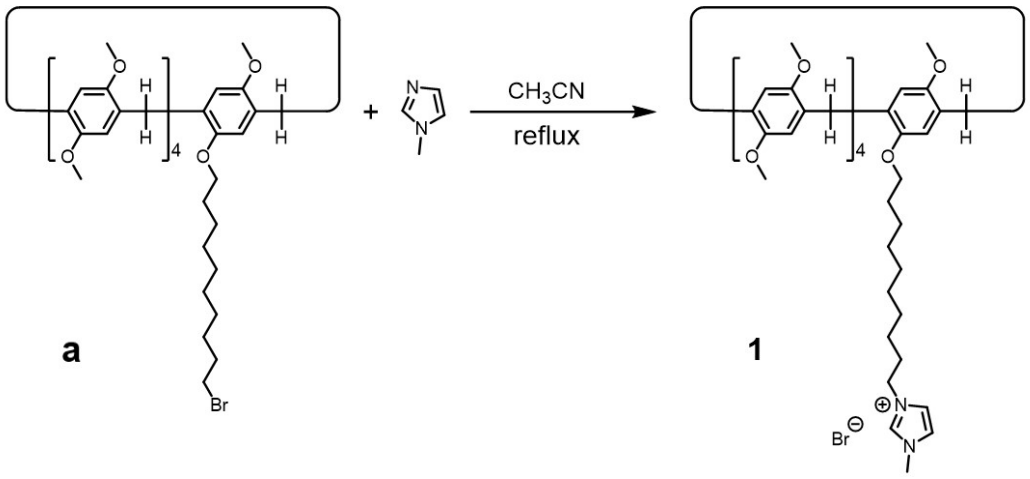

***Scheme S1**. Synthetic route to **1**.*

Compound **a** (0.48 g, 0.50 mmol) and 1-methylimidazole (0.21 g, 2.5 mmol) were added to acetonitrile (50.0 mL). The solution was refluxed 24 h. The solvent was evaporated and the residue was purified by chromatography on silica gel (dichloromethane/methanol, v/v 10:1) to give **1** as a white solid. Mp: 149−151 ℃ The ^{1}H NMR spectrum of **1** is shown in Fig. S1. ^{1}H NMR (600 MHz, CD_3CN, 298 K) δ (ppm): δ 8.40 (s, 1H), 7.31 (s, 1H), 7.24 (s, 1H)，6.91−6.88 (m, 10H), 3.89−3.87 (m, 3H), 3.81 (s, 2H), 3.73−3.68 (m, 39H), 1.83−1.79 (m, 2H), 1.63−1.61 (m, 2H), 1.55−1.52 (s, 2H), 1.39−1.36 (s, 10H), 1.20 (s, 2H). The ^{13}C NMR spectrum of **1** is shown in Figure S2. ^{13}C NMR (125 MHz, $CDCl_3$, 298 K) δ (ppm): 151.09, 151.07, 151.05, 151.03, 151.01, 150.43, 136.90, 129.49, 129.47, 129.41, 129.39, 129.36, 129.34, 129.33, 124.36, 122.97, 115.02, 114.08, 114.05, 114.00, 113.92, 113.89, 69.24, 56.21, 5618, 56.15, 50.11, 44.62, 36.74, 30.08, 30.03, 29.80, 29.48, 26.89, 26.71. HRESIMS is shown in Fig. S3: *m/z* 957.52545 $[M - Br]^{+}$.

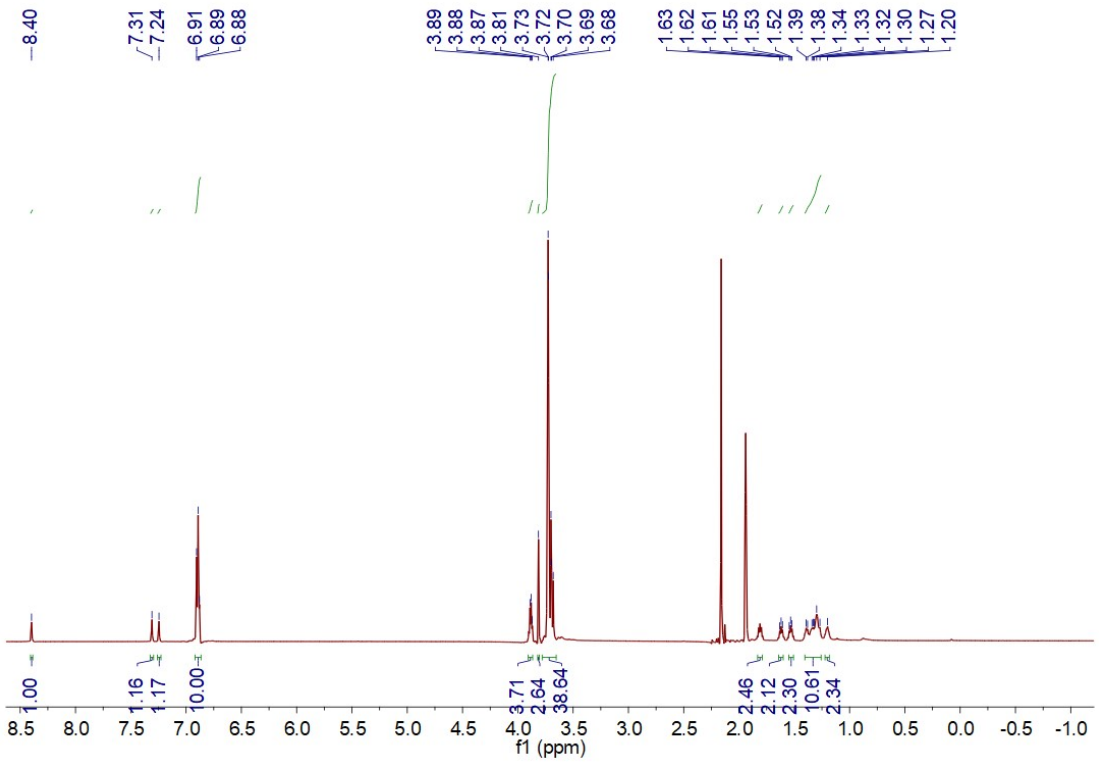

Figure S1. ^{1}H NMR spectrum (600 MHz, CD_3CN, 298 K) of **1**.

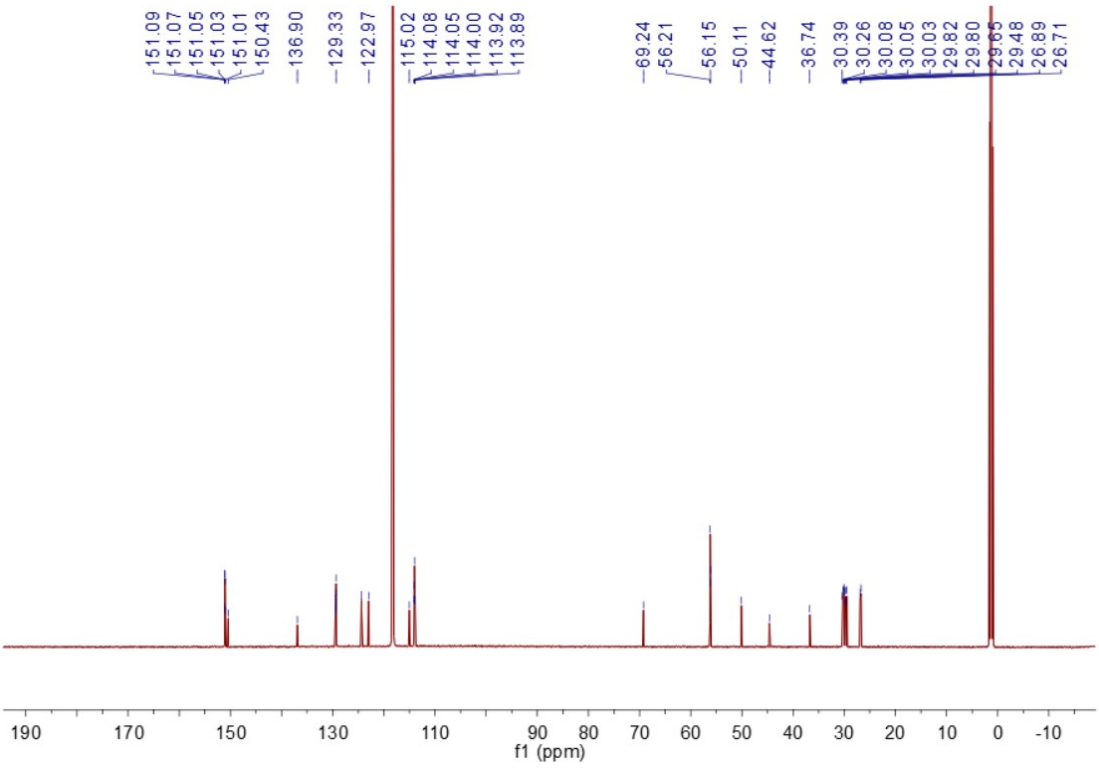

Figure S2. ^{13}C NMR spectrum (125 MHz, CD_3CN, 298 K) of **1**.

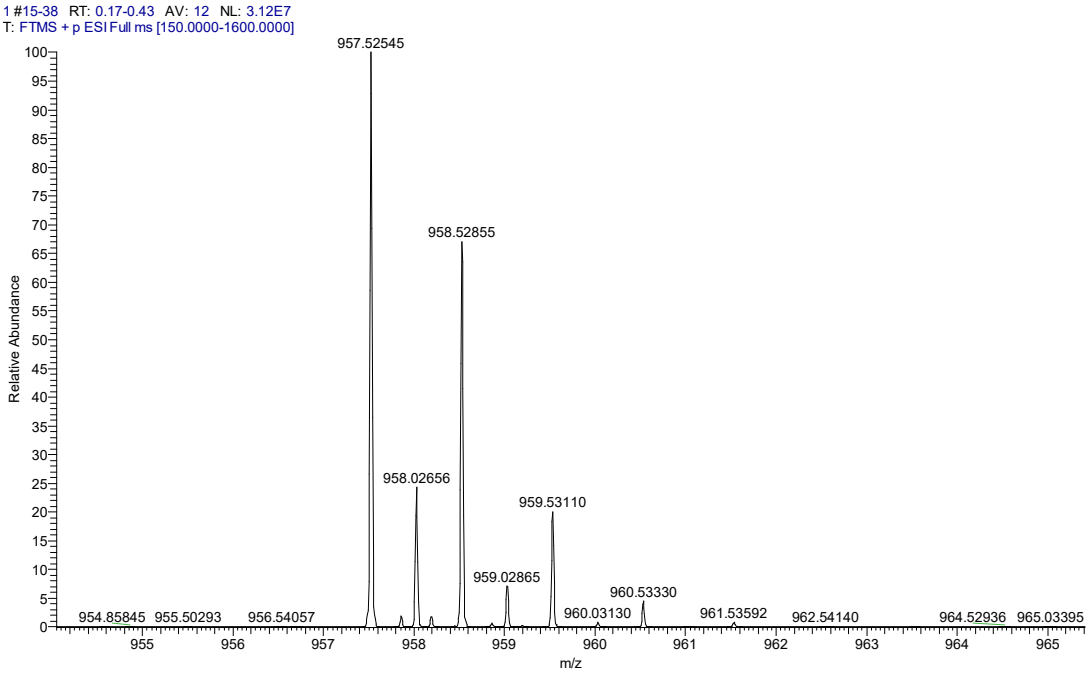

Figure S3. High-resolution mass electrospray ionization mass spectrum of **1**. Main peak: *m/z* 957.52545 $[M - Br]^+$ (100%).

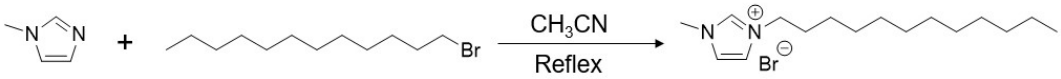

Scheme S2. *Synthetic route to compound **G**.*

1-methylimidazole (1.65 g, 20.0 mmol) and 1-bromododecane (15.0 g, 60.0 mmol) were added to acetonitrile (100.0 mL). The solution was refluxed 12 h. The solvent was evaporated and the residue was purified by chromatography on silica gel (dichloromethane/methanol, v/v 20:1) to give **G** as a white solid. Mp: 45−47 ℃. The ^{1}H NMR spectrum of G is shown in Fig. S4. ^{1}H NMR (600 MHz, $CDCl_3$, 298 K) δ (ppm): δ 10.36 (s, 1H), 7.51 (s, 1H), 7.36−7.35 (m, 1H) ，4.30−4.28 (m, 2H), 4.11 (s, 3H), 2.05 (s, 1H), 1.91−1.86 (m, 2H), 1.30−1.21 (m, 19H), 0.86−0.83 (m, 3H). The ^{13}C NMR spectrum of **G** is shown in Figure S5. ^{13}C NMR (125 MHz, $CDCl_3$, 298 K) δ (ppm): δ 138.28, 123.01, 121.45, 77.25, 77.04, 76.83, 50.36, 36.87, 29.49, 26.28, 22.70, 14.15, 1.04. HRESIMS is shown in Fig. S6: *m/z* 251.24799 $[M - Br]^+$.

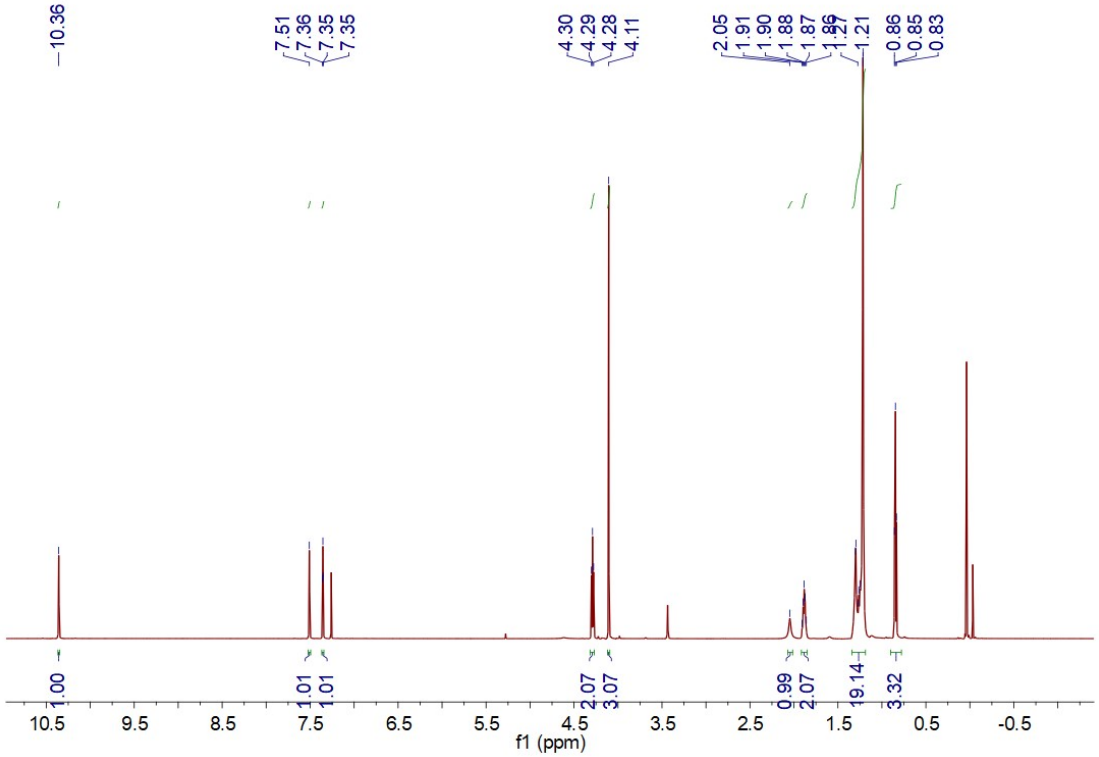

Figure S4. ^{1}H NMR spectrum (600 MHz, $CDCl_3$, 298 K) of **G**.

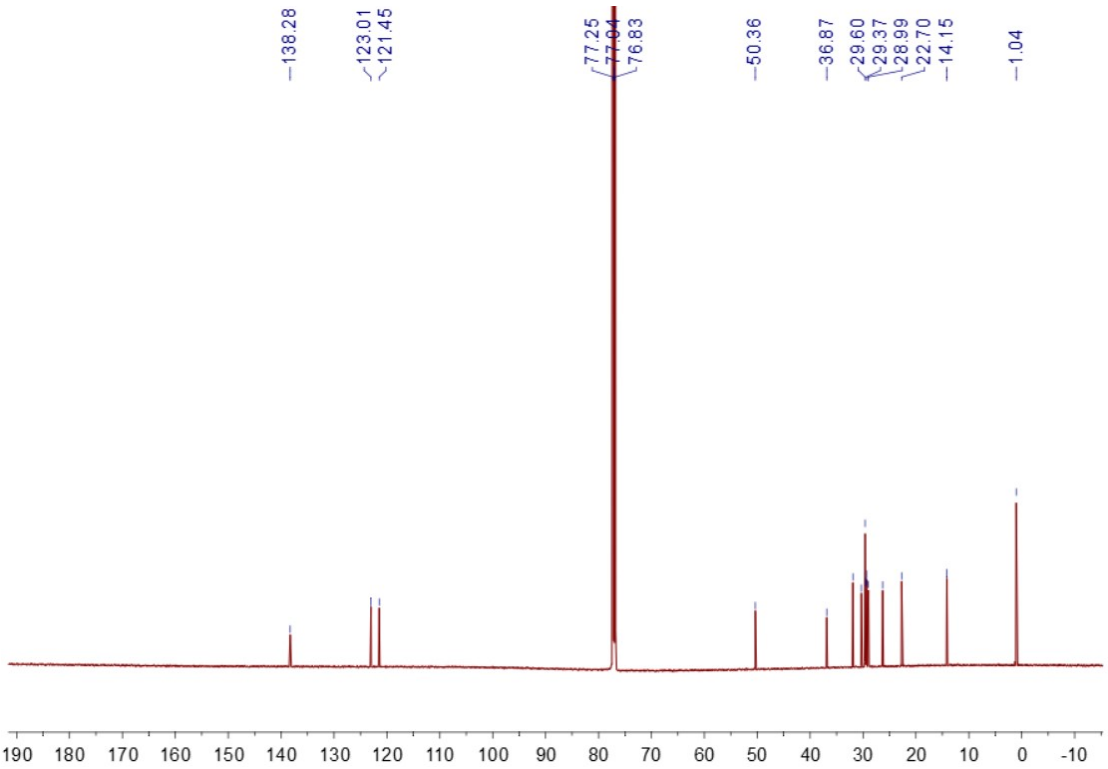

Figure S5. ^{13}C NMR spectrum (125 MHz, $CDCl_3$, 298 K) of **G**.

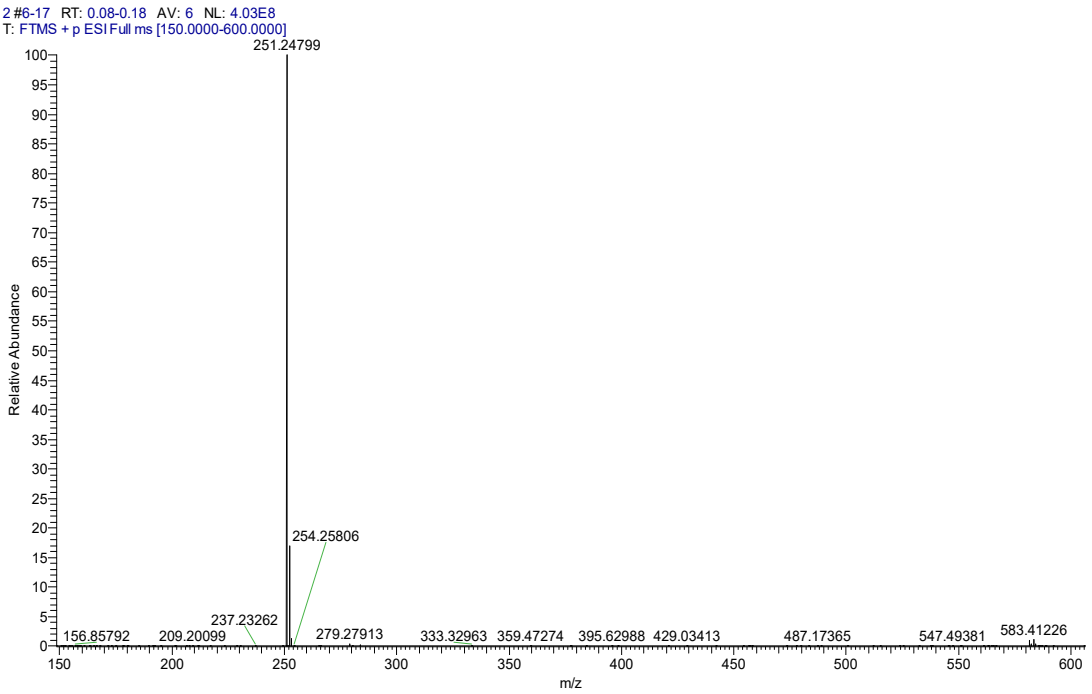

Figure S6. High-resolution mass electrospray ionization mass spectrum of **G**. Main peak: *m/z* 251.24799 $[M - Br]^+$ (100%).

*3. Study on the complexation between **H** and model guest **G***

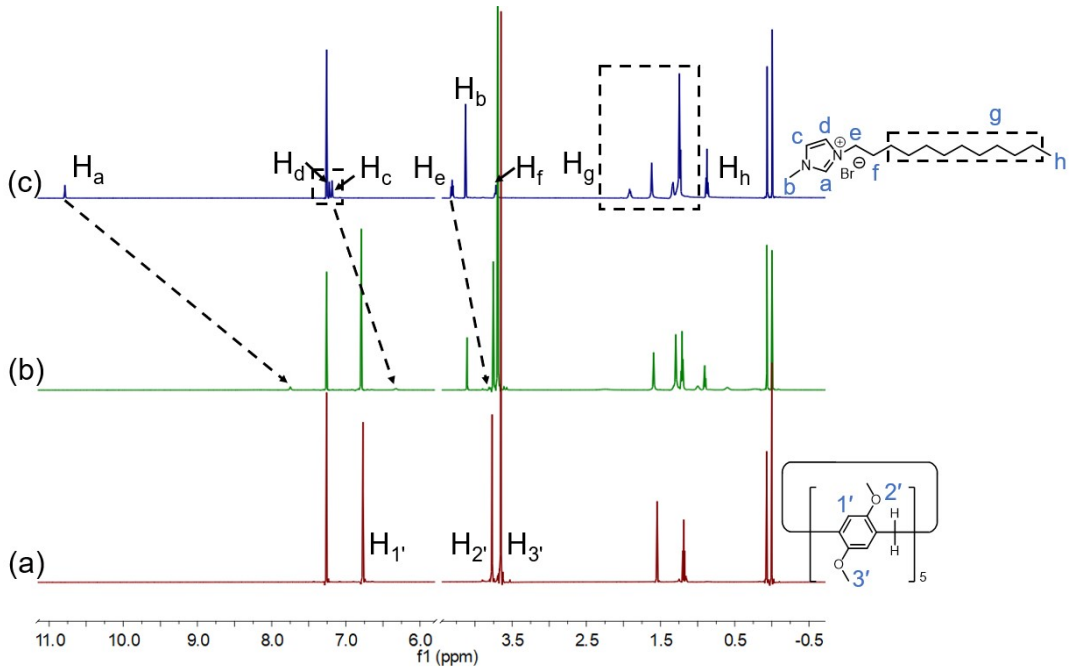

Figure S7. Partial ^{1}H NMR spectra (600 MHz, $CDCl_3$, 298 K) of (a) **H** (5.00 mM), (b) **H** (5.00 mM) and **G** (5.00 mM), (c) **G** (5.00 mM).

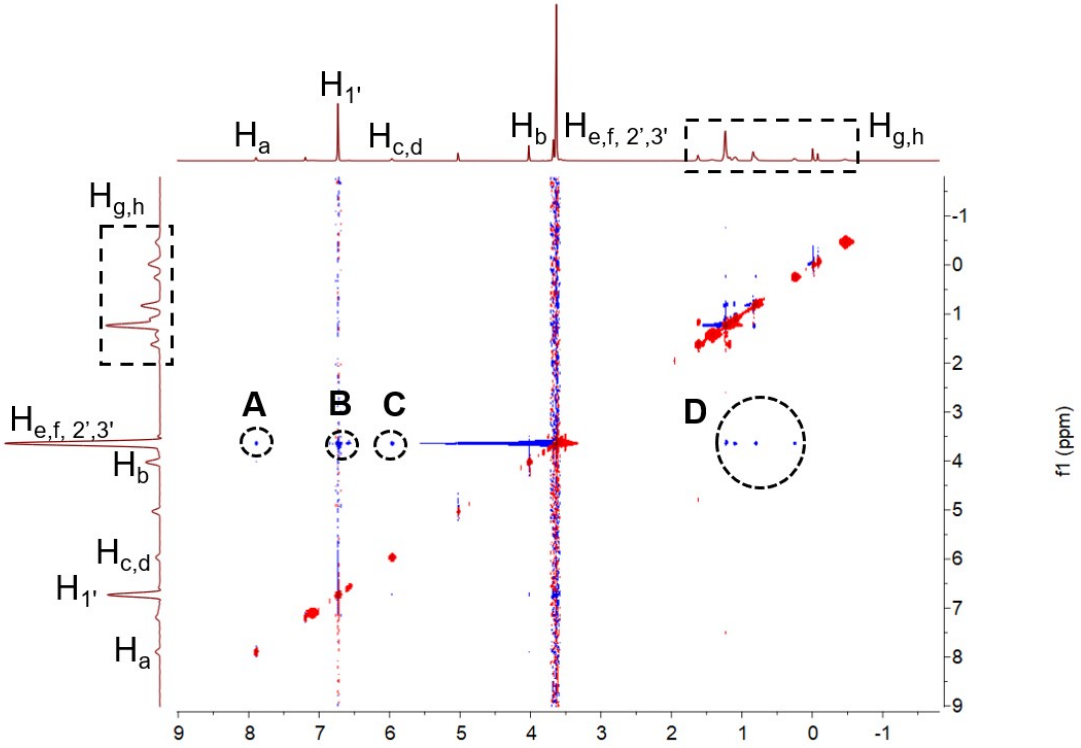

Figure S8. Partial 2D NOESY spectra ($CDCl_3$, 293 K, 600 MHz) of the mixture of **H** (20.0 mM) and **G** (20.0 mM).

To determine the stoichiometry and association constant between **H** and **G**, ^{1}H NMR titration was done with solutions which had a constant concentration of **G** (1.00 mM) and different concentrations of **H**. By a non-linear curve-fitting method, the association constant between the **H** and **G** was calculated. By a mole ratio plot, a 1:1 stoichiometry was obtained for this system.

The non-linear curve-fitting was based on the equation:

$$\Delta\delta = (\Delta\delta_\infty/[H]_0)\ (0.5[G]_0 + 0.5([H]_0 + 1/K_a) - (0.5([G]_0^2 + (2[G]_0(1/K_a - [H]_0)) + (1/K_a + [H]_0)^2)\ 0.5)) \quad \text{(Eq. S1)}$$

wherein $\Delta\delta$ is the chemical shift change of H_c on **G** at $[G]_0$, $\Delta\delta_\infty$ is the chemical shift change of H_c when the guest is completely complexed, $[G]_0$ is the fixed initial concentration of the guest, and $[H]_0$ is the varying concentration of **H**.

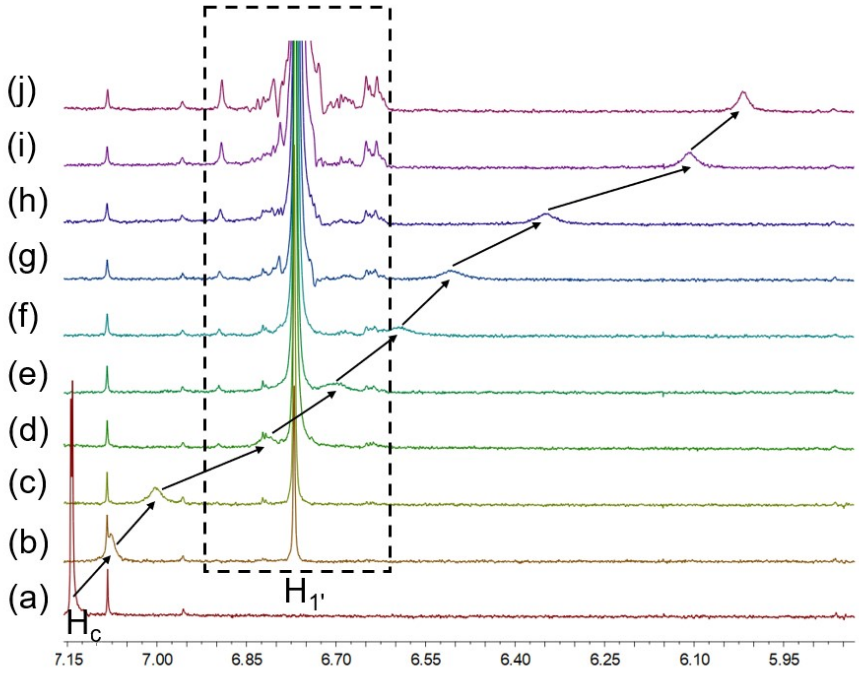

Figure S9. Partial ^{1}H NMR spectra (600 MHz, $CDCl_3$, 298 K) of **G** at a concentration of 1.00 mM with different concentrations of **H**: (a) 0.00 mM; (b) 0.10 mM; (c) 0.20 mM; (d) 0.57 mM; (e) 0.83 mM; (f) 1.15 mM; (g) 1.45 mM; (h) 2.13 mM; (i) 4.01 mM; (j) 5.17 mM.

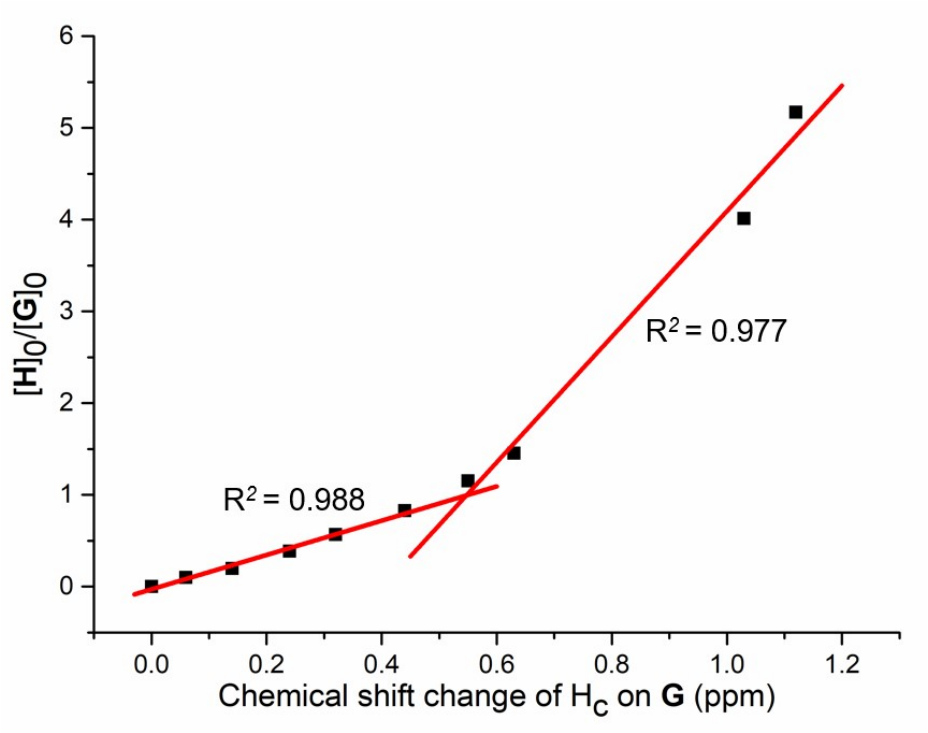

Figure S10. Mole ratio plot for the complexation between **H** and **G**, indicating a 1:1 stoichiometry.

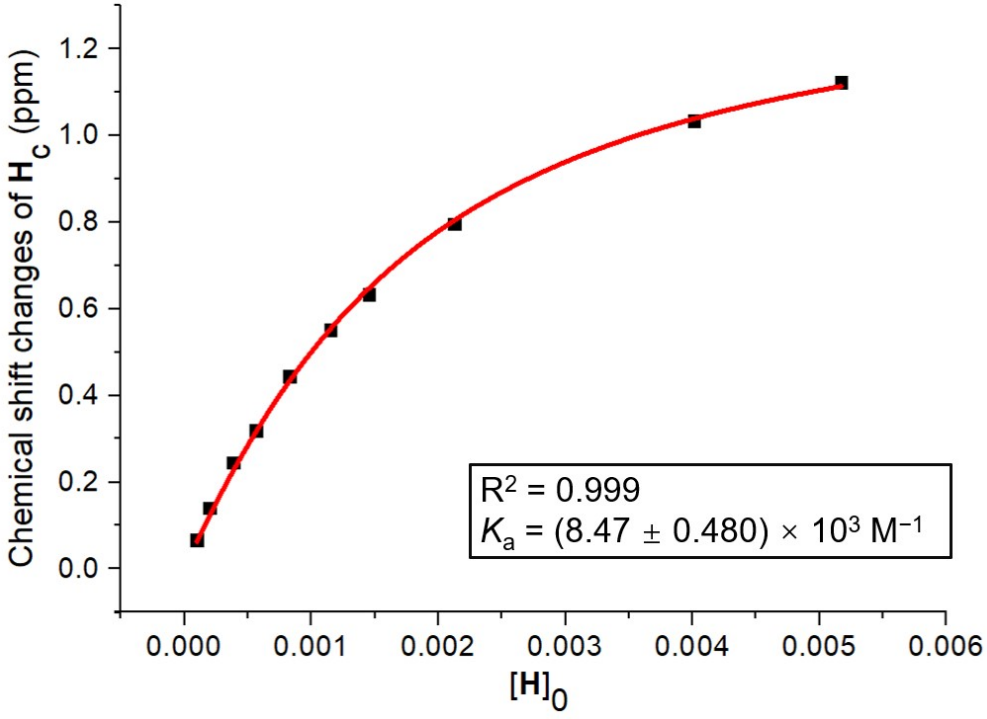

Figure S11. The chemical shift changes of H_c on **G** upon addition of **H**. The red solid line was obtained from the non-linear curve-fitting using Eq. S1.

*4. Partial DOSY NMR spectra of **1** at different concentrations.*

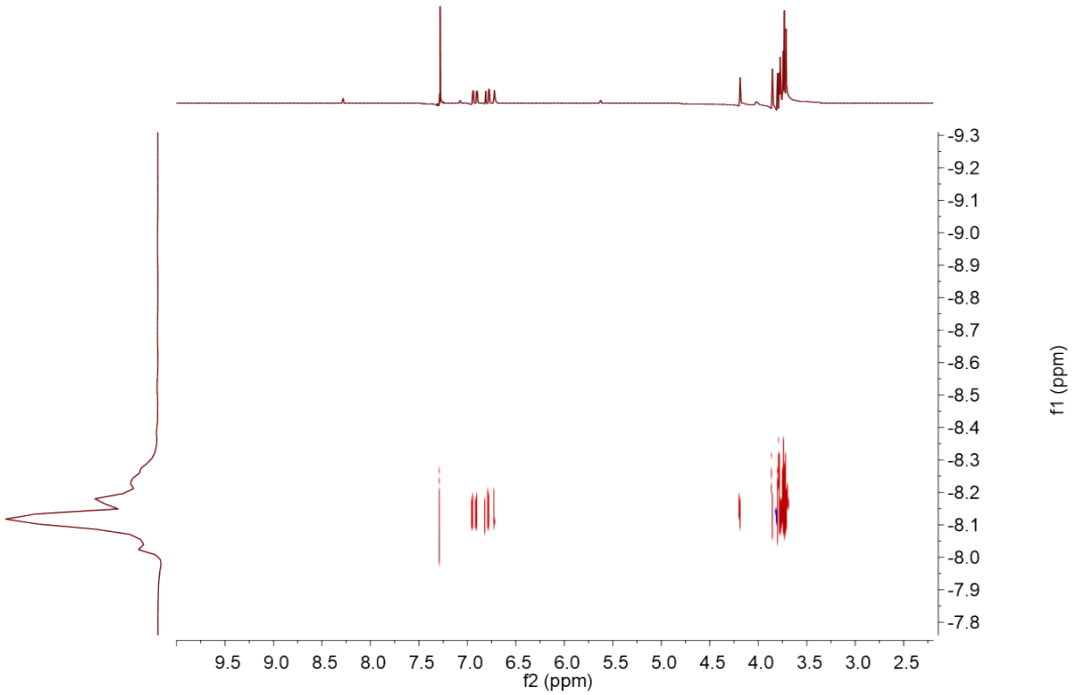

Figure S12. DOSY NMR spectrum (600 MHz, $CDCl_3$, 298 K) of **1** at 2.50 mM.

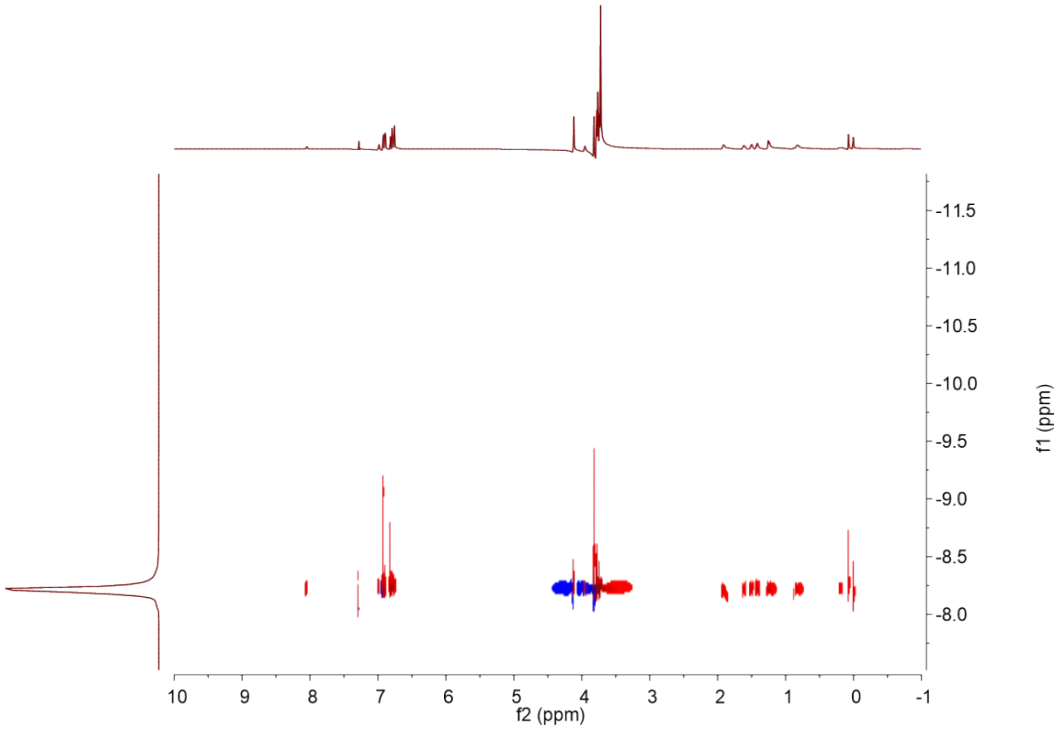

Figure S13. DOSY NMR spectrum (600 MHz, $CDCl_3$, 298 K) of **1** at 40.0 mM.

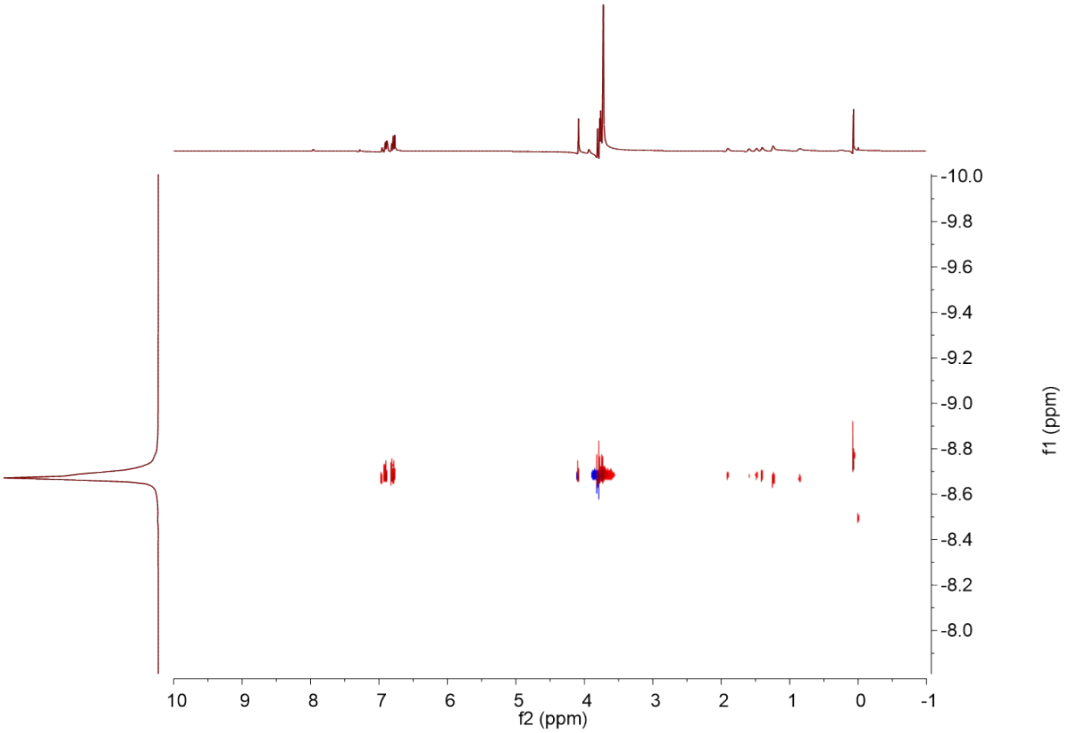

Figure S14. DOSY NMR spectrum (600 MHz, $CDCl_3$, 298 K) of **1** at 70.0 mM.

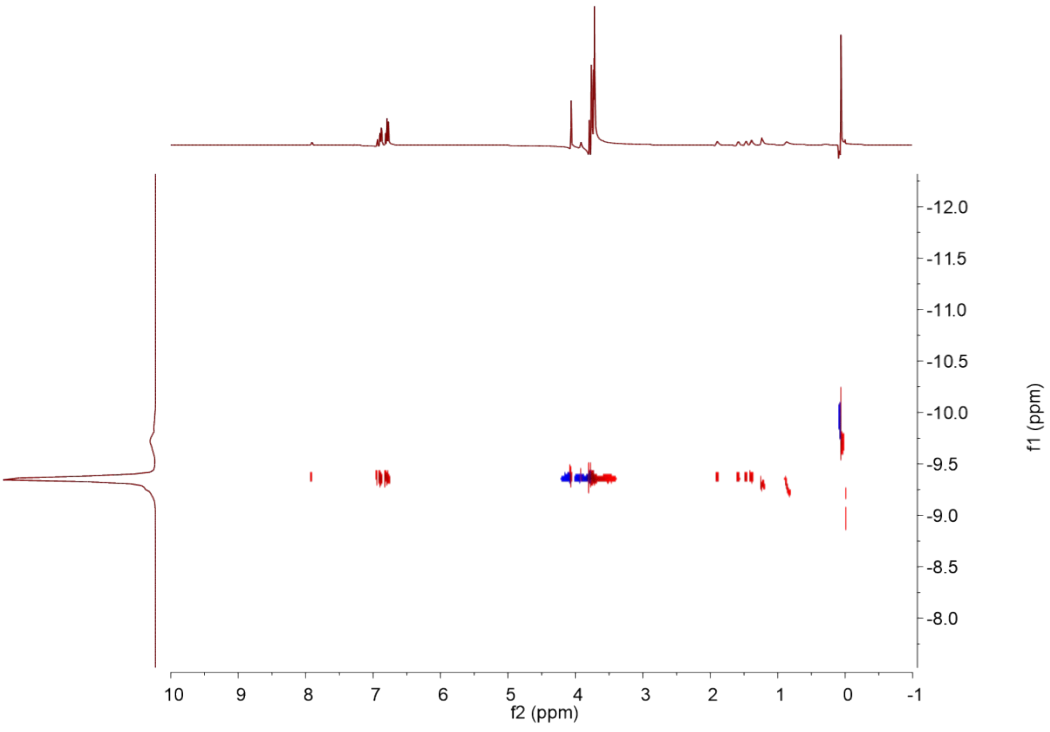

Figure S15. DOSY NMR spectrum (600 MHz, $CDCl_3$, 298 K) of **1** at 100 mM.

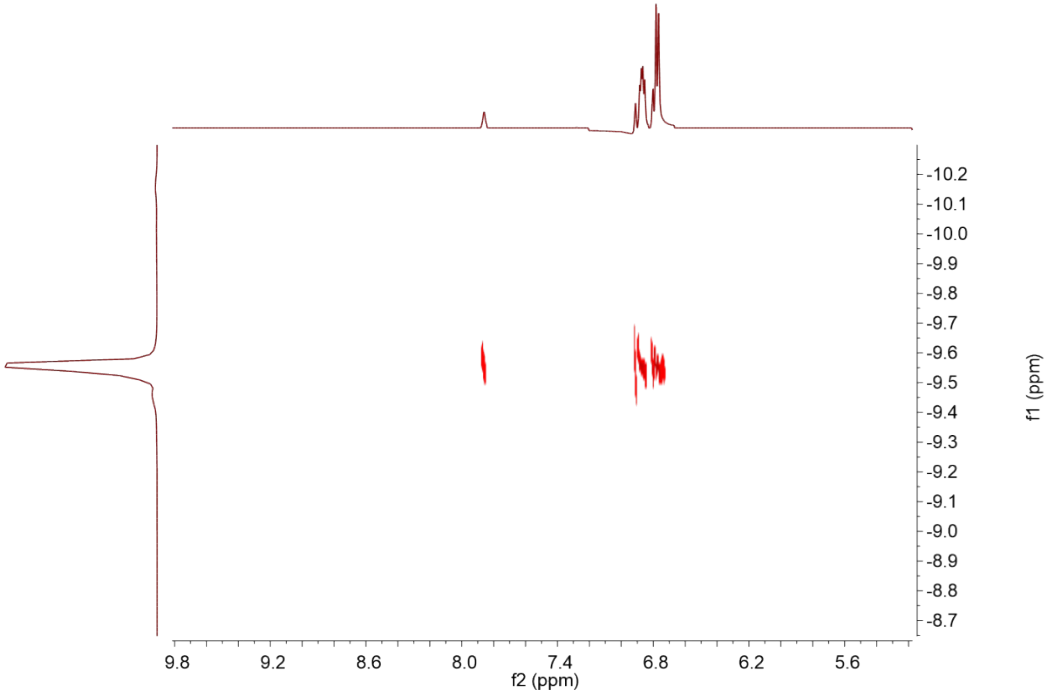

Figure S16. DOSY NMR spectrum (600 MHz, $CDCl_3$, 298 K) of **1** at 150 mM.

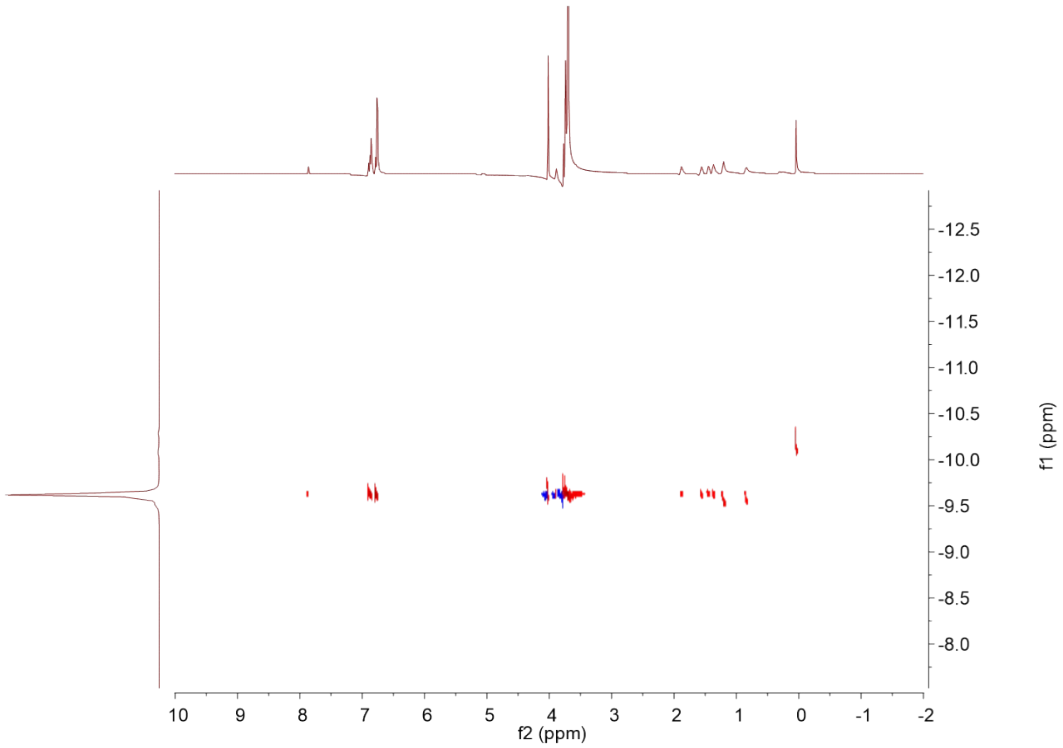

Figure S17. DOSY NMR spectrum (600 MHz, $CDCl_3$, 298 K) of **1** at 200 mM.

*5. Log–log plot of specific viscosity of monomer **1** versus the monomer concentration at 298 K.*

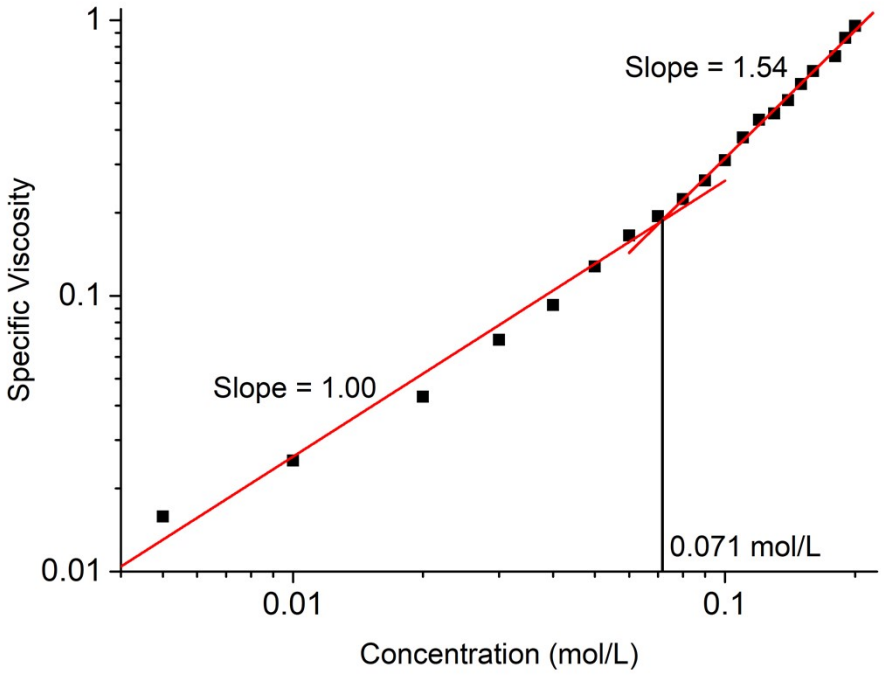

Figure S18. Log–log plot of specific viscosity of monomer **1** versus the monomer concentration at 298 K.

*6. Partial DOSY NMR spectra of **SPN**.*

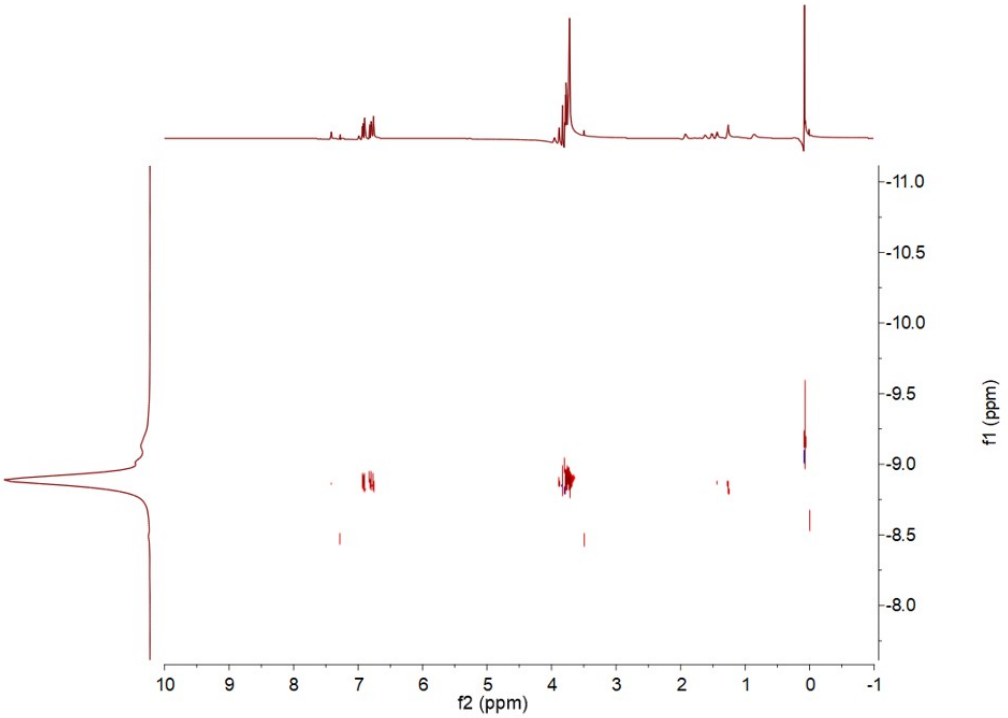

Figure S19. DOSY NMR spectrum (600 MHz, $CDCl_3$, 298 K) of **SPN** at 40.0 mM of **1**.

*7. DLS experiments of **LSP** and **SPN**.*

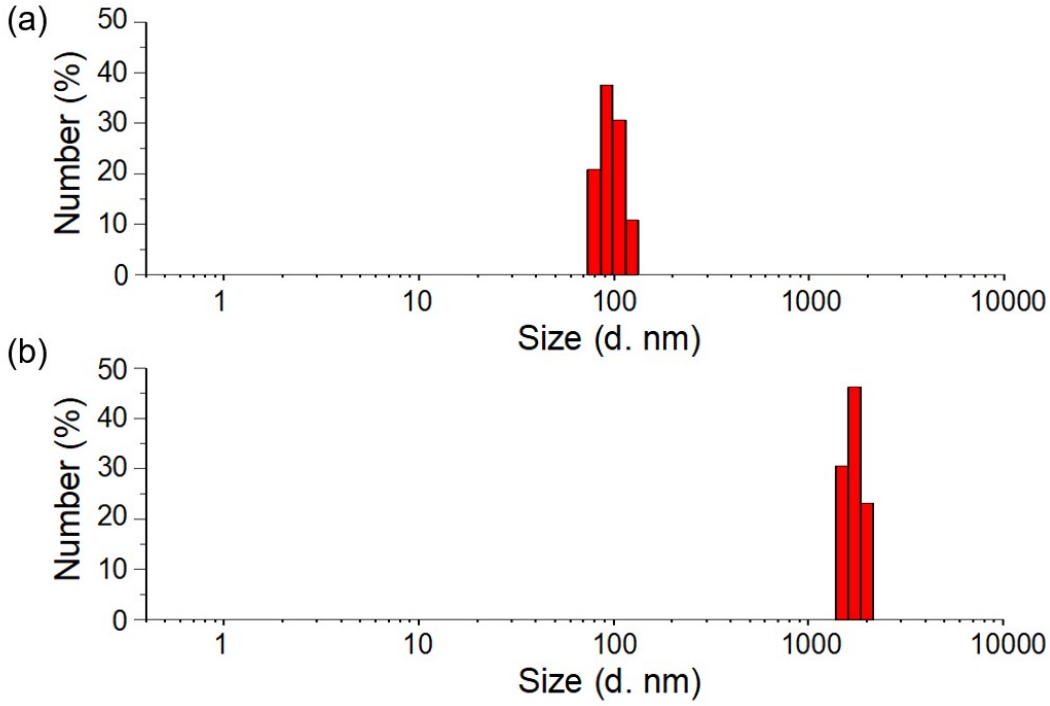

Fig. S20 DLS results of (a) **LSP** (10.0 mM of **1**); (b) **SPN** (10.0 mM of **1**) in chloroform.

*8. Partial [1]H NMR spectra and DOSY NMR spectra of **1** + TBAI.*

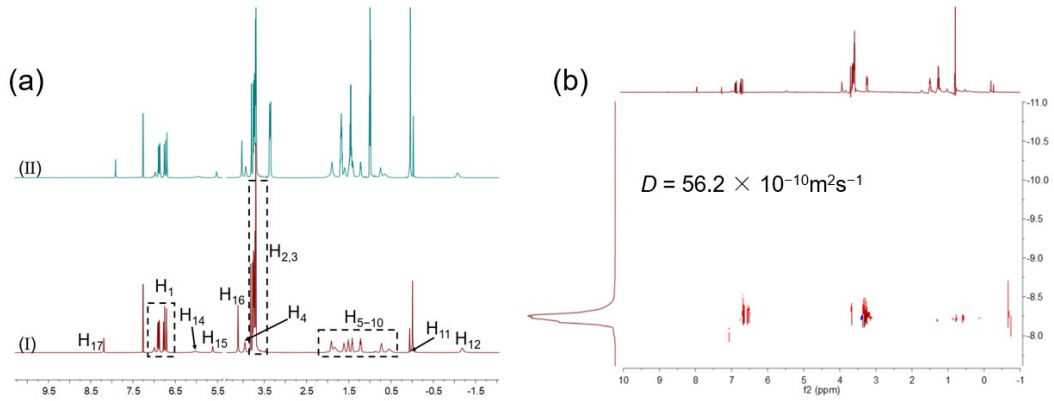

Fig. S21 (a) Partial [1]H NMR spectra (600 MHz, $CDCl_3$, 298 K) of (I) **1** at a concentration of 40.0 mM; (II) after addition 1.00 eq. TBAI to I; (b) DOSY NMR spectrum (600 MHz, $CDCl_3$, 298 K) of **1** + TBAI (40.0 mM).

9. Removal of dyes experiments

The efficiency of dye removal (in %) by the adsorbent **SPN** was determined by the following equation[S3]:

$$\% \text{ dye removal efficiency} = \frac{c_0 - c_t}{c_0} \times 100\% \quad \text{(Eq. S2)}$$

where c_0 (mg L^{-1}) was the initial concentration of dyes solution, c_t (mg L^{-1}) was the residual concentration of dyes solution in the presence of gel at any sample time t (min).

Meanwhile, the amount of dyes bound to the adsorbent were determined by the following equation[S4]:

$$q_t = \frac{c_0 - c_t}{c_A} \quad \text{(Eq. S3)}$$

where q_t (mg g^{-1}) was the amount of dyes adsorbed per gram of adsorbent at time t (min), c_0 (mg L^{-1}) and c_t (mg L^{-1}) were the initial and residual concentrations of dyes in the stock solutions and filtrates, c_A (g L^{-1}) was the concentration of adsorbent.

The adsorption kinetic process was described by pseudo-second-order adsorption model, shown as the following equation[S5]:

$$\frac{t}{q_t} = \frac{t}{q_e} + \frac{1}{k_A q_e^2} \quad \text{(Eq. S4)}$$

where q_t (mg g^{-1}) and q_e (mg g^{-1}) were the amount of dyes adsorbed at time t (min) and at equilibrium time, k_A (g mg^{-1} min^{-1}) was the apparent adsorption rate constant.

The Langmuir adsorption isotherm was shown in the following equation[S6]:

$$\frac{c}{q_e} = \frac{1 + kc}{kq_{max}}$$

where q_e (mg g^{-1}) was the mass amount of the pollutant adsorbed at equilibrium, q_{max} (mg g^{-1}) was the maximum adsorption amount of the adsorbent at equilibrium, c (mg L^{-1}) was the residual pollutant concentration at equilibrium, and k (L mg^{-1}) was the equilibrium constant.

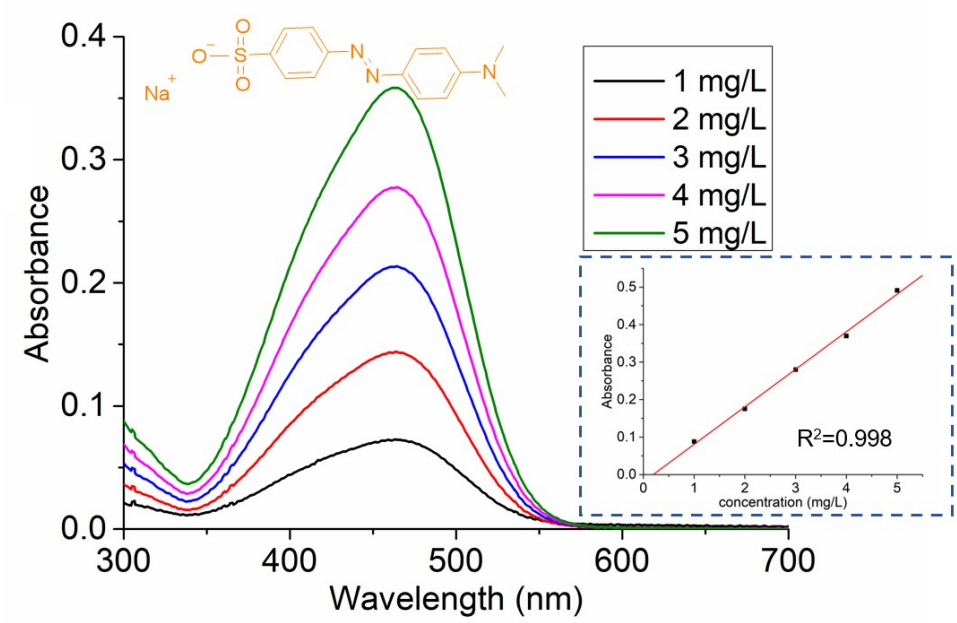

Figure S22. Concentration-dependent UV−Vis spectrum changes of methyl orange, insert: Standard curve measured by UV−vis of methyl orange.

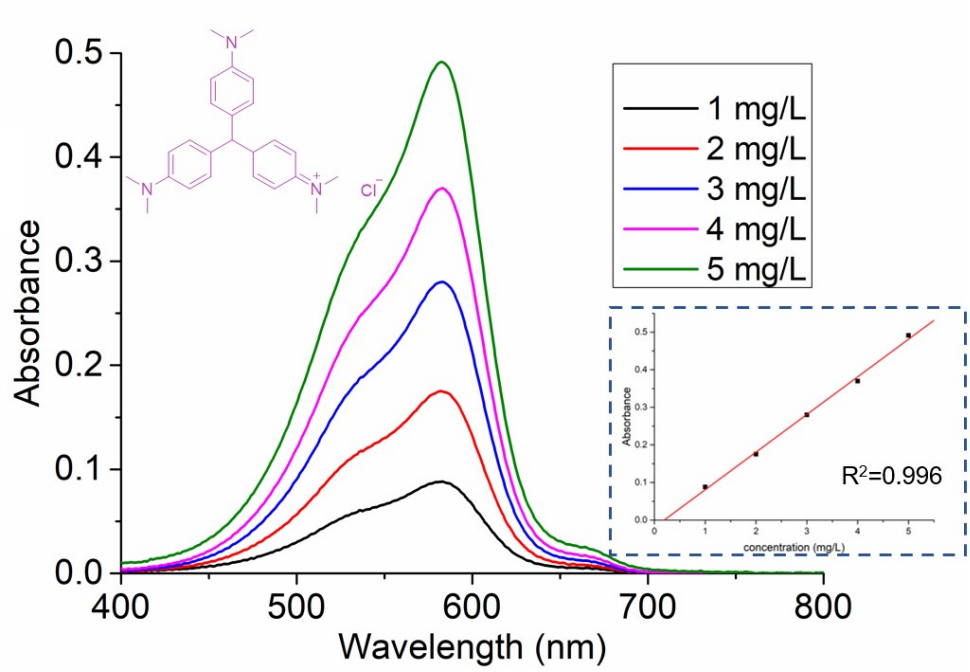

Figure S23. Concentration-dependent UV−Vis spectrum changes of methyl violet, insert: Standard curve measured by UV−vis of methyl violet.

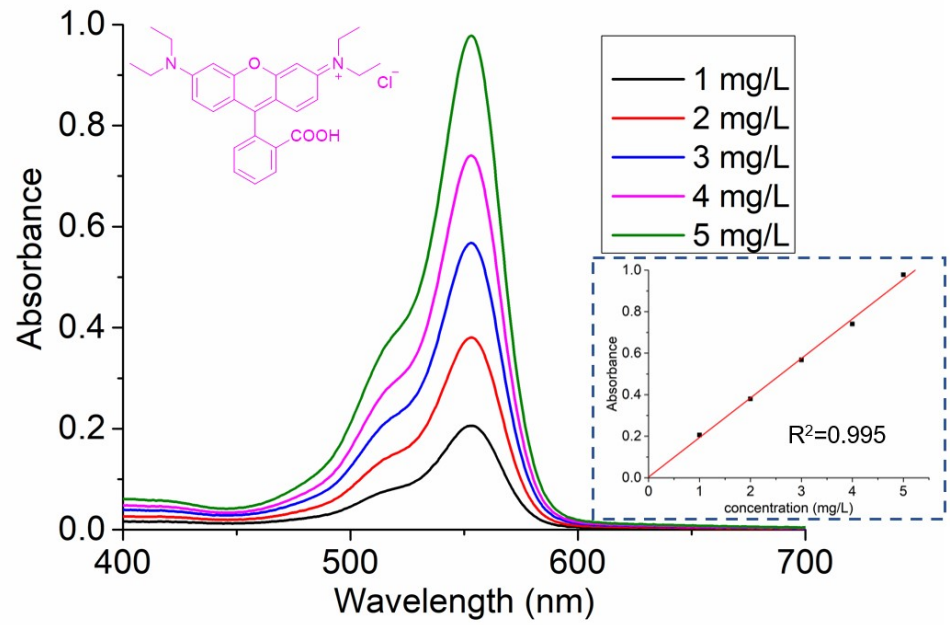

Figure S24. Concentration-dependent UV−Vis spectrum changes of rhodamine B, insert: Standard curve measured by UV−vis of rhodamine B.

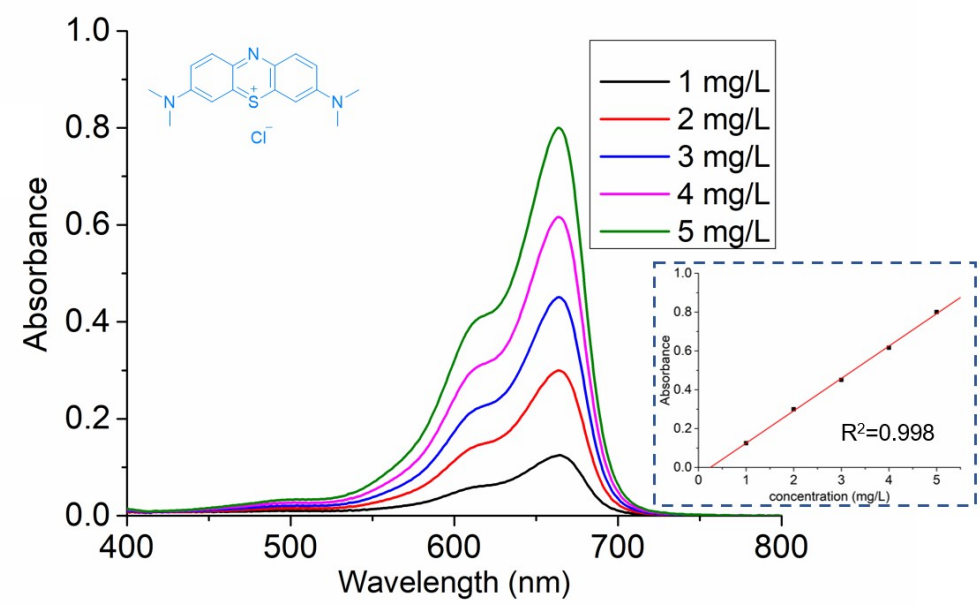

Figure S25. Concentration-dependent UV−Vis spectrum changes of methylene blue, insert: Standard curve measured by UV−vis of methylene blue.

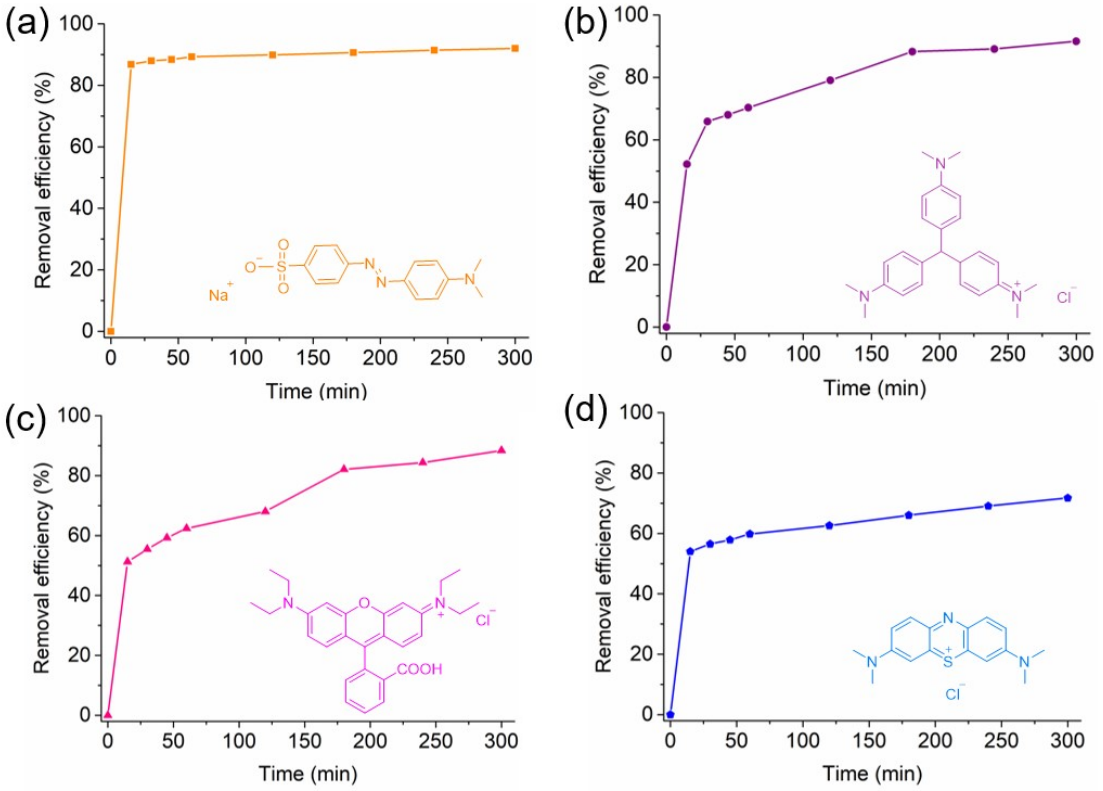

Figure S26. Time-dependent removal efficiency of (a) methyl orange, (b) methyl violet, (c) rhodamine B, (d) methylene blue.

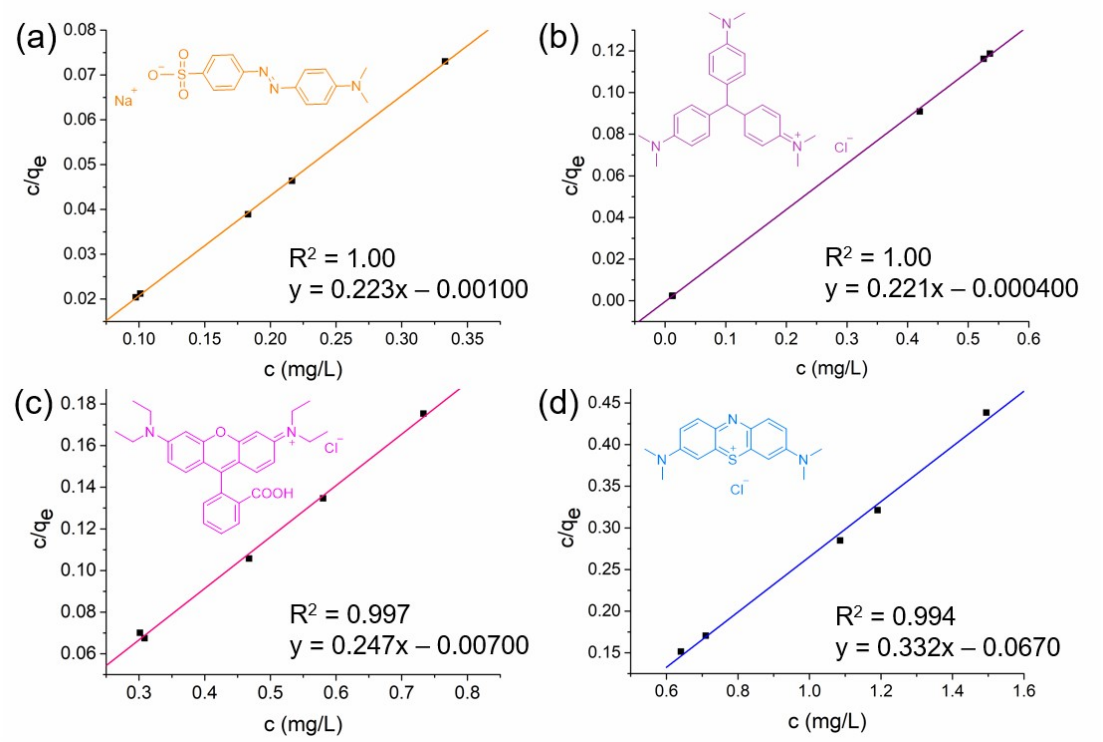

Figure S27. The Langmuir isotherm of (a) methyl orange, (b) methyl violet, (c) rhodamine B, (d) methylene blue adsorption by **SPN**.

*10. Stability text of **SPN***

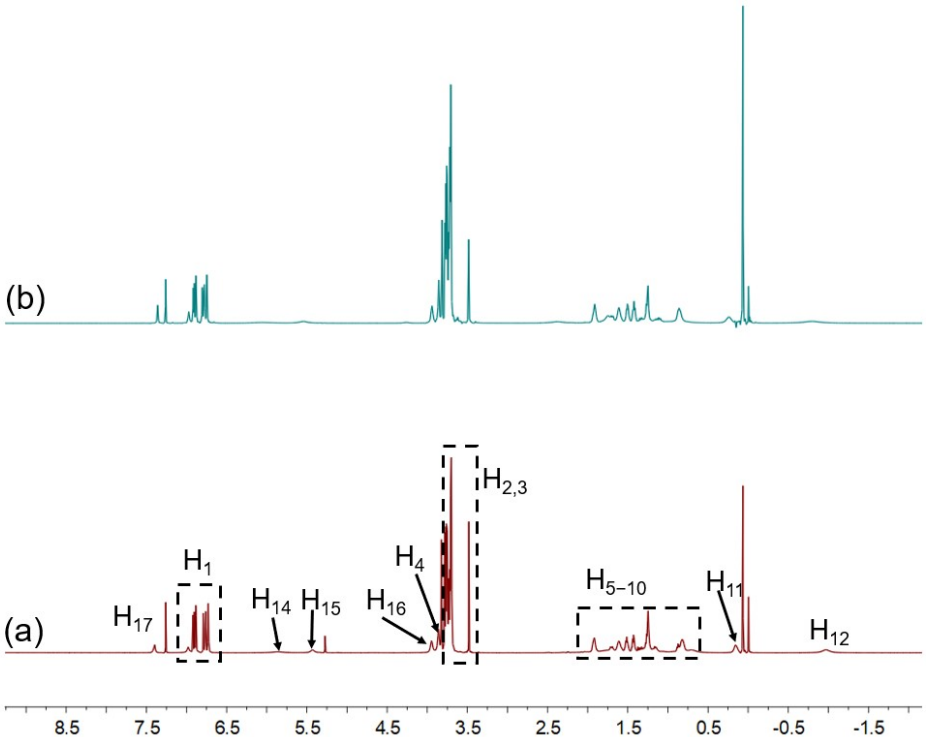

Figure S28. ^{1}H NMR spectra (600 MHz, $CDCl_3$, 298 K) of (a) **SPN** and (b) **SPN** in water for 24 hours and was dried in vacuum.

References

S1. Z. Zhang, C. Han, G. Yu and F. Huang, *Chem. Sci.*, 2012, **3**, 3026−3031.

S2. T. Ogoshi, S. Kanai, S. Fujinami, T. Yamagishi and Y. Nakamoto, *J. Am. Chem. Soc.*, 2008, **130**, 5022−5023.

S3. A. Meng, J. Xing, Z. Li and Q. Li, *ACS Appl. Mater. Interfaces*, 2015, **7**, 27449−27457.

S4. W. Zhang, Y. Zhang and Y. Liu, *Chem Asian J*, 2021, **16**, 2321−2327.

S5. Y. S. Ho and G. McKay, *Process Biochem.*, 1999, **34**, 451−465.

S6. M. T. Yagub, T. K. Sen, S. Afroze and H. M. Ang, *Adv. Colloid Interface Sci.*, 2014, **209**, 172−184.